Cellular uptake of multilayered capsules produced with natural and genetically engineered biomimetic macromolecules

Rui R. Costa [a,b], Alessandra Girotti [c,d], Mercedes Santos [c,d], F. Javier Arias [c,d], João F. Mano [a,b,*], J. Carlos Rodríguez-Cabello [c,d]

[a] 3B's Research Group—Biomaterials, Biodegradables and Biomimetics, University of Minho, Headquarters of the European Institute of Excellence of Tissue Engineering and Regenerative Medicine, AvePark, Zona Industrial da Gandra, S. Cláudio do Barco, 4806-909 Caldas das Taipas—Guimarães, Portugal
[b] ICVS/3B's, PT Government Associated Laboratory, Braga/Guimarães, Portugal
[c] G.I.R. Bioforge, University of Valladolid, Edificio I+D, Paseo de Belén, 11, 47011 Valladolid, Spain
[d] Networking Research Center on Bioengineering, Biomaterials and Nanomedicine (CIBER-BBN), Valladolid, Spain

A B S T R A C T

Multilayered microcapsules of chitosan and biomimetic elastin-like recombinamers (ELRs) were prepared envisaging the intracellular delivery of active agents. Two ELRs containing either a bioactive RGD sequence or a scrambled non-functional RDG were used to construct two types of functionalized polymeric microcapsules, both of spherical shape ~4 μm in diameter. Cell viability studies with human mesenchymal stem cells (hMSCs) were performed using microcapsule/cell ratios between 5:1 and 100:1. After 3 and 72 h of co-incubation, no signs of cytotoxicity were found, but cells incubated with RGD-functionalized microcapsules exhibited higher viability values than RDG cells. The internalization efficacy and bioavailability of encapsulated DQ-ovalbumin were assessed by monitoring the fluorescence changes in the cargo. The data show that surface functionalization did not significantly influence internalization by hMSCs, but the bioavailability of DQ-ovalbumin degraded faster when encapsulated within RGD-functionalized microcapsules. The microcapsules developed show promise for intracellular drug delivery with increased drug efficacy.

Keywords:
Cellular uptake
Multilayer capsules
Layer-by-layer
Biomaterials

1. Introduction

In the field of drug delivery, there has been much interest in developing active agent nano- and micro-carriers, such as micelles, liposomes, polymersomes and polymer capsules [1–4]. Such devices may be used in the release control of encapsulated biomolecules and to increase their efficacy by delivering them to the location where they are needed most. In particular, nanostructured nano- and micro-capsules made using layer-by-layer (LbL) strategies have been studied to encapsulate and deliver drugs in a controlled manner [5–9]. The principle behind LbL adsorption lies in the existence of intermolecular interactions that potentiate attraction among distinct polymer chains. Some examples include electrostatic contacts, hydrophobic interactions and hydrogen bonding, which drive the assembly of layers of a few nanometers onto a surface [10–12]. With this simple and versatile technique, robust coatings can be assembled on bidimensional templates and even complex three-dimensional substrates. For example, multilayer microcapsules have already been proposed as biosensors and as drug carriers—including stem cell differentiation promoters—with tunable release kinetics dependent on the number of layers or on external stimuli [13–17].

Multilayer capsules may encapsulate and deliver bioactive agents to cells or tissues by conventional mechanisms of release to the biological environment [18] or by digestion within the cells themselves [19]. The latter possibility is particularly interesting: delivering drugs to the intracellular environment, where the whole metabolic machinery is found, ensures that large amounts are delivered to the target tissue, ensuring their high efficacy. Moreover, it could be possible to circumvent undesirable side effects to the surrounding cells or tissues resulting from premature drug leakage. Dendrimers, micelles and biodegradable nanoparticles have been developed for the intracellular delivery of bioactive agents [20–23]. In comparison, multilayer-coated capsules present several advantages that are not often found in other conventional

fabrication techniques: (i) they can be prepared in mild conditions, allowing large amounts of sensitive or easily denatured biological molecules [24] and even cells [25] to be encapsulated; (ii) it is possible to encapsulate drugs with low water solubility [6]; (iii) the release rate can be controlled better by varying the number of layers and their composition [26]; and (iv) the shell can provide a high degree of functionality by selecting biofunctional building blocks that may participate in biological mechanisms [27].

The primary objective of the present work was the design of multilayer microcapsules made of natural and nature-inspired biomaterials exhibiting bioactive sequences for intracellular drug delivery: namely, chitosan (CHI) and elastin-like recombinamers (ELRs) were used as building blocks for multilayer shells, assembled on spherical particles of calcium carbonate. CHI is a well-known polycationic polysaccharide of marine origin, exhibiting biocompatibility, adhesiveness and non-toxicity, as well as bacteriostatic, fungistatic, antimicrobial and hemostatic activities [28]. ELRs, a recombinant type of elastin-like polymer, are temperature-responsive and biomimetic polypeptides. They are soluble in aqueous media below a critical transition temperature (T_t), but undergo phase separation above it [29]. Their recombinant and modular nature is perhaps their most attractive property, because their physicochemical properties can be tuned, and introducing specific relevant amino acid domains can extend their physiological functionality [30,31]. LbL adsorption can be performed using ELRs alongside polysaccharides such as CHI and alginate by resorting to strong electrostatic interactions and the stabilizing effect of weaker hydrophobic interactions [32].

In the present study, human mesenchymal stem cells (hMSCs) were co-incubated with microcapsules made with an ELR exhibiting the cell adhesion motif arginine–glycine–aspartic acid (RGD). RGD is a motif of the human structural protein fibronectin, and is the minimal sequence required for recognition by cell adhesion receptor integrins [33]. Using RGD has previously enhanced the internalization of nano-/micro-particles [34–36]. However, such assessment has been often made with controls that do not exhibit any sort of functionalization. Therefore, in addition to RGD, the present authors also constructed microcapsules with an ELR exhibiting a non-functional scrambled RDG sequence (referred to as $RDG^{(-)}$, for the sake of distinction), instead of completely eliminating the functional layer. To the present authors' knowledge, this is the first time that the internalization efficacy of RGD-functionalized LbL microcapsules has been compared with a microcapsule type that substitutes the bioactive group with a non-functional analogue.

The synthesized microcapsules were characterized in terms of morphology and cytotoxicity toward hMSCs. The internalization efficacy of microcapsules was quantified by flow cytometry in order to identify the existence—or absence—of a receptor-mediated uptake. Capsules loaded with DQ-ovalbumin enabled an assessment of its degradation stage by monitoring fluorescence changes inside the cells.

2. Materials and methods

2.1. Materials

Medium molecular weight CHI (Ref. 448877), sodium carbonate anhydrous (Na_2CO_3, Ref. 222321) and ethylenediaminetetraacetic acid (EDTA) (Ref. E9884) were purchased from Sigma–Aldrich. CHI was purified in a series of filtration and precipitation in water and ethanol steps, adapted from the method described elsewhere [37], followed by freeze-drying. The degree of deacetylation was determined as 82% by ^{1}H-NMR. Calcium chloride ($CaCl_2$) was purchased from VWR (Ref. 1.02378.0500). Two custom-made ELRs containing either RGD or $RDG^{(-)}$ peptide sequences were purchased from Technical Protein Nanobiotechnology (Spain) (a schematic representation can be found in Supplementary Figure 1, in Appendix B). Molecular weight and amino acid composition of the acquired batches were determined by matrix-assisted laser desorption/ionization time-of-flight mass spectroscopy and amino acid content analysis, respectively, and can be found elsewhere [32]. DQ-ovalbumin (Ref. D12053) was obtained from Invitrogen. Rhodamine B isothiocyanate (Ref. 283924) was purchased from Sigma–Aldrich.

Paraformaldehyde (Ref. P6148), Triton X-100 (Ref. T9284) and Accutase™ (Ref. A6964) were purchased from Sigma–Aldrich. The hMSCs from human adipose tissue (Ref. R7788-115), its basal medium, Dulbecco's modified Eagle's medium (DMEM, Ref. 31966-021), fetal bovine serum (FBS Ref. 16000-044), penicillin streptomycin solution (ref SV30010), trypsin-EDTA (Ref. SV30010), Dulbecco's phosphate buffered saline (DPBS) (Ref. 14190-136), 4-(2-hydroxyethyl)-1-piperazineethanesulfonic acid (HEPES) (Ref. 15630049), Trypan Blue stain 0.4% (Ref. 15250061), Alexa Fluor 488 phalloidin (Ref. A12379), LIVE/DEAD® Viability/Cytotoxicity Kit, for mammalian cells (Ref. L3224), Alamar Blue® (Ref. DAL1025) and DAPI (Ref. D21490) were supplied by Invitrogen. All cell culture plastic ware and consumables were acquired from NUNC.

2.2. Measurement of the charges

The zeta (ζ)-potentials of the ELRs were determined using Nano-ZS equipment from Malvern (UK), at 25 °C. Aqueous solutions of each ingredient in phosphate buffered saline (PBS) (pH = 7.4) were used, with a concentration of 300 $\mu g \cdot ml^{-1}$.

2.3. Synthesis of calcium carbonate sacrificial templates

Aqueous solutions of Na_2CO_3 and $CaCl_2$ were prepared with a concentration of 1 M. Typically, the co-precipitation of both solutions was performed by adding 1 ml of Na_2CO_3 solution, followed by 1 ml of $CaCl_2$ to 4 ml of ultrapure water (Milli-Q) under heavy stirring for 30 s. The stirring was then stopped, and the newly synthesized calcium carbonate ($CaCO_3$) microparticle suspension was left to precipitate and react for 15 min. The supernatant was removed, and the particles were washed three times with 0.15 M sodium chloride (NaCl) adjusted to pH 5.5. To produce microcapsules preloaded with protein cargo, the medium where the co-precipitation occurs consisted of an aqueous solution of DQ-ovalbumin with a concentration of 160 $\mu g \cdot ml^{-1}$. Unless otherwise stated, all changes of solutions after the template synthesis reaction and during the construction of microcapsules were made by leaving the particle suspension precipitating for 10 min, followed by removal of the supernatant and replacement with the next solution—polymeric or washing.

2.4. Construction of the multilayer shells and microcapsule formation

The $CaCO_3$ sacrificial templates were immersed alternately in solutions of CHI and of ELR (300 $\mu g \cdot ml^{-1}$, pH 5.5, 0.15 M NaCl) for 10 min under mild stirring. Each adsorption step was followed by three steps of washing with 0.15 M NaCl, pH 5.5: to disaggregate the substrates, the first washing step was accompanied by four sequential ultrasound pulses of 3 s each, while the subsequent steps were only rinsing. This process was repeated until two CHI/ELR bilayers were assembled. After the construction of the multilayers, the $CaCO_3$ core was dissolved using EDTA at 0.2 M, pH 5.5. From this point on, the precipitation of the microcapsules was aided by centrifugation (1000 rpm, 25 min) and ultrasound pulses timed as described above. The newly formed hollow microcapsules

were then washed once with EDTA (0.2 M, pH 7.4) and four times with ultrapure water. The microcapsules were stored at room temperature for 24 h (maximum) in ultrapure water until use. In the case of microcapsules intended for cellular assays—loaded with DQ-ovalbumin—DMEM was used for washing and storage instead of water. The microcapsule production yield resulting from the mixture of 1 ml of Na_2CO_3 and $CaCl_2$ was estimated by microscopy observation to be $\sim 1.1 \times 10^6$ microcapsules.

2.5. Characterization of the polysaccharide/polypeptide microcapsules

Confocal laser scanning microscopy (CLSM; Olympus FV1000, Germany) was used to observe rhodamine-dyed multilayer shells. For this, microcapsules were immersed for 10 min in a solution of rhodamine B (10^{-6} M) after their synthesis. All samples were stabilized at 37 °C and observed under hydrated conditions. Fluorescence intensity profiles of three distinct microcapsules were plotted using ImageJ software (provided by NIH, version 1.47v). The morphology of DQ-ovalbumin-loaded microcapsules was determined using environmental scanning electron microscopy (ESEM) (FEI Quanta 200FEG). Then, 2.2×10^4 microcapsules suspended in 200 μl of H_2O were placed on top of a silicon wafer (1 cm^2) and dried overnight at 37 °C before analysis. The samples were placed inside the equipment in a platform with a 20° tilt. Observations of microcapsules were made from three independent syntheses.

2.6. Cell culture

The hMSCs were cultured in DMEM supplemented with 10% FBS and 100 $U \cdot ml^{-1}$ penicillin, 0.1 $mg \cdot ml^{-1}$ streptomycin, replaced every 2 days and maintained at 37 °C in a 5% CO_2 humidified environmental chamber. Near-confluence cells (passages 2–6) were harvested after enzymatic treatment with trypsin/EDTA or Accutase™ and suspended in culture medium. Cell counts were evaluated using a standard Trypan Blue exclusion assay. Then, $3 \times 10^3 cell \cdot cm^{-2}$ were seeded on the diverse surfaces and incubated for 24 h in standard conditions. At the start of the experiments involving co-incubating hMSCs with microcapsules, the culture medium was refreshed by serum-free medium (to avoid interference with the RGD-mediated microcapsule capture) containing a suspension of CHI/ELR microcapsules. After 3 h co-incubation of CHI/ELR microcapsules, the cultures were maintained for longer times by supplementing the microcapsule suspension with additional fresh medium, to reach the final serum concentration of 2% FBS.

2.7. Cell viability assays

Metabolic activity was evaluated by Alamar Blue® and cell viability by LIVE/DEAD® assays. The relative number of hMSCs metabolically active within each experimental condition was evaluated by the Alamar Blue® assay, according to the manufacturer's guidelines. Briefly, 24 h after cell seeding, cells were washed with DPBS and then $(CHI/ELR\text{-}RGD)_2$ or $(CHI/ELR\text{-}RDG^{(-)})_2$ microcapsules in serum-free culture medium were added in ratios varying between 5 and 100 microcapsules per cell. After 3 and 72 h of co-incubation, fluorimetric reduction of 10% Alamar Blue® reagent in culture medium was measured with a microtiter plate reader (SpectraMax M2e Molecular Devices). Non-treated cells were used as a positive control, and their fluorescence was considered as 100% of cell viability. Values reported reflect means ± standard error (SE) of four samples from four independent cell culture viability experiments after 3 or 72 h of co-incubation.

Cell viability was also examined by LIVE/DEAD® assays. Ten microcapsules per cell of each CHI/ELR microcapsule type were added to the cell culture. The ratio of microcapsules per cell was selected after the results of cell viability assays. In this assay, the co-incubation with calcein AM and ethidium homodimer-1 allows the cytoplasm of live cells (with esterase cleavage of calcein accompanied by green fluorescence) and dead cells (which compromised membranes enable to stain nucleic acids with red fluorescence) to be distinguished. LIVE/DEAD® assays were carried out for different time points (0, 72 and 240 h) according to the manufacturer's specifications.

2.8. Cell analysis by flow cytometry

After 1.5×10^5 hMSCs had been seeded in 25 cm^2 flasks and cultured as described above ("Cell culture" subsection), $(CHI/ELR\text{-}RGD)_2$ or $(CHI/ELR\text{-}RDG^{(-)})_2$ microcapsules were added in a microcapsule/cell ratio of 10:1 and co-incubated for 72 h. The cell cultures dissociated by Accutase™ treatment—specially developed for gentle and effective cell dissociation—were washed, counted, suspended in DPBS, 25 mM HEPES, 5% FBS, and analyzed in a flow cytometer Gallio (Beckman Coulter). The assay was repeated three times.

2.9. Internalization and intracellular processing experiments

The hMSCs were seeded on circular cover glasses (diameter 10 mm; Thermo Scientific CB00100RA1) deposited in 48-well plates and incubated for 24 h in standard conditions. $(CHI/ELR\text{-}RGD)_2$ or $(CHI/ELR\text{-}RDG^{(-)})_2$ microcapsules were added to the culture. After 3 or 72 h of co-incubation, samples were washed three times with DPBS.

Samples for microscopy analysis—confocal, phase-contrast, epifluorescence and differential interference contrast (DIC) microscopy (Nomarski)—were fixed in 4% paraformaldehyde for 10 min, permeabilized with 0.2% Triton X-100, and stained with DAPI. Confocal microscopy (Leica Microsystems, Heidelberg GmbH, microscope confocal Leica SP5) was used to analyze microcapsules inside the cells. Z-series were performed with a Z-step of 1 μm. Images of each fluorophore and phase contrast were overlaid to obtain a multilayer image, using ImageJ (provided by NIH, version 1.47v). Bright-field and fluorescence microscopy were performed in a NIKON Eclipse Ti fluorescence microscope, equipped with a digital camera system (Digital sight DS-2MBWc), using blue, green and red filters.

2.10. Statistical analysis

The influence of microcapsule/cell ratio on cell viability and internalization efficacy by flow cytometry was analyzed using one-way analysis of variance and the post test of Bonferroni. All treatment-related effects were considered to be statistically significant for $P < 0.05$. All data were analyzed using GraphPad Prism 6.0 (GraphPad Software, Inc., La Jolla, CA).

3. Results

$CaCO_3$ microparticles—entrapping DQ-ovalbumin or not—were coated with two bilayers of CHI and an ELR exhibiting either RGD or $RDG^{(-)}$. ELR-RGD and ELR-$RDG^{(-)}$ exhibited ζ-potential values of −5.7 ± 1.2 mV and −6.3 ± 1.2 mV in PBS, respectively. After coating, hollow microcapsules—henceforth referred to as $(CHI/ELR\text{-}RGD)_2$ or $(CHI/ELR\text{-}RDG^{(-)})_2$—were produced by incubating them in EDTA, which led to the dissolution of the sacrificial template. In order to confirm that the microcapsule synthesis was successful, they were evaluated by CLSM and SEM. Several CHI/ELR microcapsules of both types were stained with rhodamine and observed in CLSM (Fig. 1A). All microcapsules showed diameters of 3–4 μm

and possessed their own individual walls and spherical morphology. In Fig. 1B, the fluorescence intensity of the wall was quantified as a function of the length of the lines drawn across the dyed microcapsules. SEM analysis of $(CHI/ELR\text{-}RGD)_2$ loaded with DQ-ovalbumin was performed to assess the dissolution of the $CaCO_3$ core and microcapsule integrity (Fig. 1C). It was thus possible to witness protein-loaded microcapsules, their morphology and surface in dehydrated conditions. As observed, wall integrity was maintained from the process of construction to the moment of their use. Moreover, the microcapsules presented folds and creases that result from (i) drying during sample preparation and (ii) the absence of a solid interior to hold the physical spherical structure, thereby pointing to the synthesis of hollow microcapsules. Similar observations were found for microcapsules made of CHI and ELR-$RDG^{(-)}$ (Fig. 1D), resembling $(CHI/ELR\text{-}RGD)_2$ microcapsules in size. Their morphology in dehydrated conditions was also similar. Furthermore, no signs of major aggregation were found for any microcapsule type (see Supplementary Figure 2 in Appendix B for a representative zoomed-out SEM micrograph), thereby demonstrating that the microcapsules produced are not only hollow, but also individually coated.

In order to assess whether this type of nanostructured microcapsule is suitable for biological applications, the in vitro viability of hMSCs was analyzed by measuring their metabolic activity in the presence of $(CHI/ELR\text{-}RGD)_2$ or $(CHI/ELR\text{-}RDG^{(-)})_2$. The dose-dependent response effect was studied for two experimental times of 3 h and 72 h. The hMSCs were co-incubated with increasing microcapsule/cell ratios within a range of 5–100 units per cell. In Fig. 2, the cell viability is represented, normalized with respect to the positive control (i.e. cells cultured without microcapsules). After 3 h (Fig. 2A) and 72 h (Fig. 2B) of co-incubation with $(CHI/ELR\text{-}RGD)_2$ microcapsules, the metabolic activity did not vary significantly with respect to the positive control in the ratio range studied. A similar trend was observed for ELR-$RDG^{(-)}$-functionalized microcapsules: for both time-points (Fig. 2C and D), there were no significant differences in metabolic activity for the various microcapsule/cell ratios. After 72 h of co-incubation (Fig. 2B and D), there was a decrease in the cellular metabolic activity incubated with both microcapsule types for the highest microcapsule/cell ratios. This decrease can be seen for a ratio higher than 50:1 for $(CHI/ELR\text{-}RGD)_2$ and 60:1 for $(CHI/ELR\text{-}RDG^{(-)})_2$ microcapsules, which may indicate a slim negative impact of the increasing number of suspended microcapsules on hMSC viability.

It was also clear that cells co-incubated with $(CHI/ELR\text{-}RDG^{(-)})_2$ microcapsules were less viable than their biofunctional analogues. For example, after incubating 10 microcapsules per cell for 72 h with hMSCs, a viability of 139% (ELR-RGD-based elements) was estimated, in comparison with 105% (ELR-$RDG^{(-)}$-based elements), accounting for a reduction of 24%. These differences in bioactivity do not account for a significant statistical difference between each microcapsule type, although the mean bioactivity values of $(CHI/ELR\text{-}RGD)_2$ are higher for all time points.

Cell viability performing LIVE/DEAD® assays was studied for a maximum of 10 days to complement the metabolic activity data (Fig. 3). Since the metabolic activity was higher for lower ratios, a standard concentration of 10 microcapsules per cell was selected during all subsequent experiments. In this way, it would be possible to keep the microcapsule/cell ratio to a minimum, while preserving high cellular metabolic activity and avoiding massive microcapsule administration. After a co-incubation period of 72 h with $(CHI/ELR\text{-}RGD)_2$ microcapsules, the green calcein staining confirmed that the cells were alive and spread on the surface (Fig. 3B). The same trend was observed for $(CHI/ELR\text{-}RDG^{(-)})_2$ microcapsules (Fig. 3E), with no visible differences between each case. To assess whether cells could remain alive after being cultured in the presence of microcapsules, complete DMEM was added after 72 h to the medium. This mixture was maintained for another 168 h to a total of 10 days of culture. As observed in Fig. 3C and F, no dead cells were encountered, indicating that hMSC viability was not affected by the foreign microcapsule components and supporting the metabolic assays results.

To show the ability of hMSCs to internalize polysaccharide/polypeptide microcapsules, in the first stage hMSCs were co-incubated with $(CHI/ELR\text{-}RGD)_2$ for 72 h. To aid this preliminary

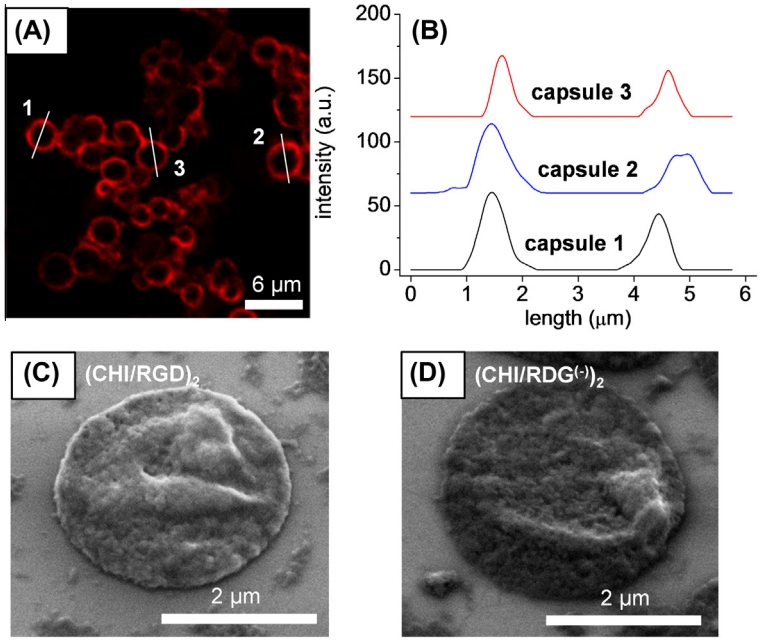

Fig. 1. (A) CLSM micrograph of several microcapsules with the walls tagged with rhodamine. Micrograph is representative of both $(CHI/ELR\text{-}RGD)_2$ and $(CHI/ELR\text{-}RDG^{(-)})_2$ microcapsules. (B) Fluorescence intensity plot profile of three individual microcapsules depicted in (A). The peaks coincide with the capsules' walls, while the plateau in-between corresponds to the hollow interior. SEM images of (C) $(CHI/ELR\text{-}RGD)_2$ and (D) $(CHI/ELR\text{-}RDG^{(-)})_2$ microcapsules containing preloaded DQ-ovalbumin, with a vertical tilt of 20°.

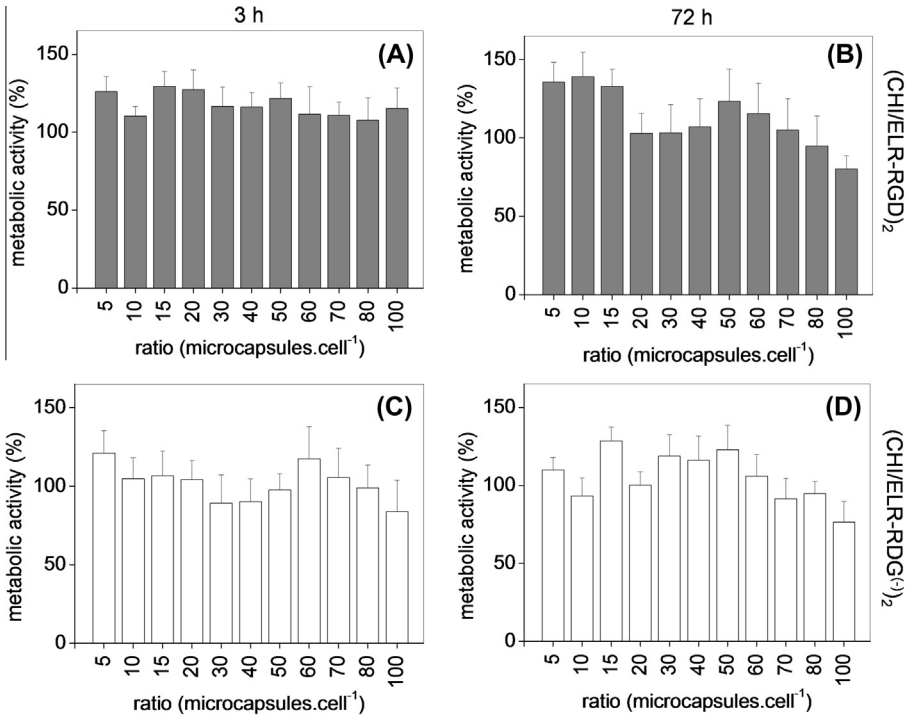

Fig. 2. Metabolic activity of hMSCs incubated with increasing ratios of (A and B) $(CHI/ELR\text{-}RGD)_2$ and (C and D) $(CHI/ELR\text{-}RDG^{(-)})_2$ microcapsules for (A and C) 3 h and (B and D) 72 h. Data represent means of four experiments, each performed in quadruplicate, normalized with respect to the positive control. Error bars represent one SD (mean + SE). No significant statistical differences were found ($P > 0.05$).

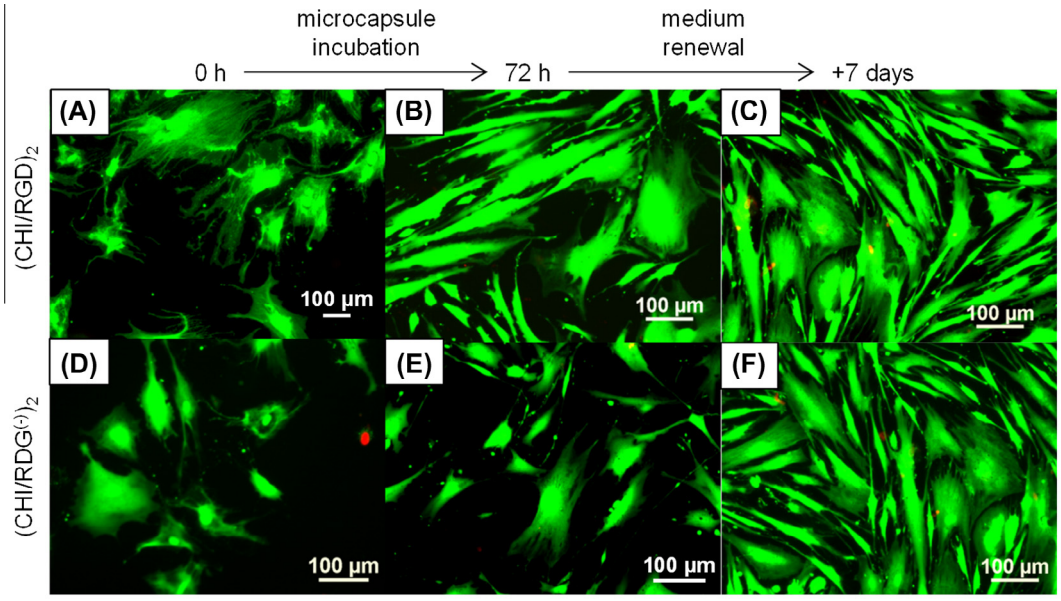

Fig. 3. Representative microphotographs of LIVE/DEAD® assay of hMSCs incubated with (A–C) $(CHI/ELR\text{-}RGD)_2$ and (D–F) $(CHI/ELR\text{-}RDG^{(-)})_2$ microcapsules at (A and D) 0, (B and E) 72 h and (C and F) 240 h times points (ratio 10:1).

assessment, the microcapsules were loaded with DQ-ovalbumin. This commercially available product is a conjugate of ovalbumin heavily labeled with BODIPY dyes. Owing to a characteristic self-quenching mechanism, it exhibits a bright red fluorescence, characterized by the close proximity of the fluorescent dyes, but it shifts to a strong green on proteolysis. This means that the internalization of the microcapsules and the intracellular processing of the cargo could be followed by fluorescence. CLSM (Fig. 4) confirmed the presence of internalized RGD-functionalized microcapsules. A yellow color (resulting from the simultaneous fluorescence emission of red and green) could be detected in different planes of the cells, evidencing that microcapsules containing DQ-ovalbumin were internalized by hMSCs. Microcapsules containing fully degraded cargo were detected inside the cells as bright green dots, indicated by the arrows (Fig. 4A). To show that microcapsules were internalized, rather than free DQ-ovalbumin (present in the medium due to premature leakage), a micrograph of two cells without fluorescence is presented in Fig. 4E (save for the DAPI-

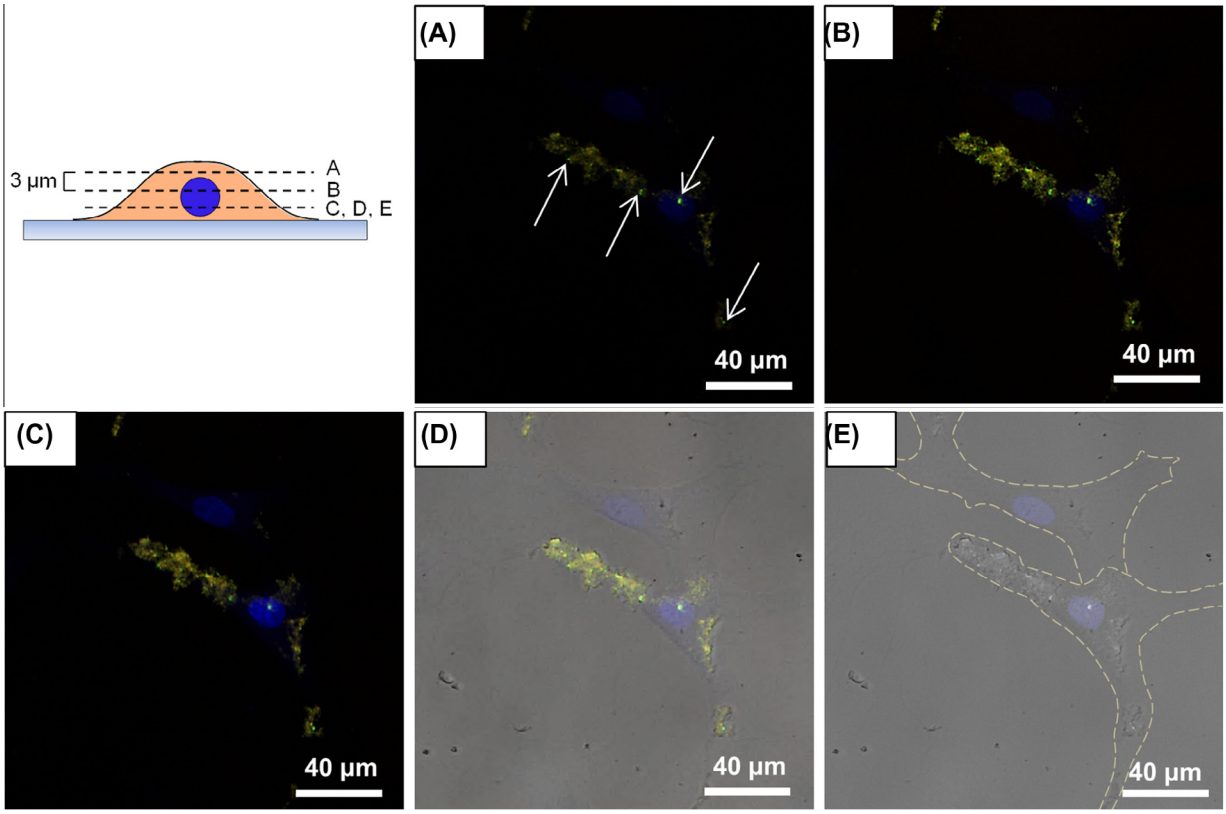

Fig. 4. Confocal microscopy of hMSCs containing $(CHI/ELR\text{-}RGD)_2$ microcapsules within their cytoplasm (ratio 10:1). The nuclei are stained with DAPI (blue), and the microcapsules loaded with DQ-ovalbumin. The schematics represent the relative position of each plane in the cell (A–C). The arrows in (A) point to bright green dots, representing fully processed DQ-ovalbumin. (D) Bright-field image merged with the fluorescence-only image in C. (E) Bright-field-only image of C, showing microcapsules in the intracellular environment of the central cell. The blue fluorescence of the stained nuclei was merged for better identification of the cells.

stained nuclei for better cell identification). The central cell shows an agglomerate of structures in the intracellular environment, corresponding to the internalized microcapsules. In comparison, the top cell did not internalize as many capsules. The depth-scanning performed during CLSM can be found in the video in Appendix B. Therefore, these results show that cellular uptake of CHI/ELR microcapsules can be achieved and that the intracellular degradation of the protein used can be followed by fluorescence microscopy.

Cells that could internalize microcapsules loaded with DQ-ovalbumin were quantified using flow cytometry (Fig. 5). For this analysis, the study of Semmling et al. [38], who performed a "flow cytometry"-based assay to analyze the uptake of polyelectrolyte capsules, was taken into consideration. Starting with the case of $(CHI/ELR\text{-}RGD)_2$ microcapsules (Fig. 5A), viable hMSC after 72 h of co-incubation are found in the area delimited by the yellow frame. Viable cells include cells that were either empty (with low side-scattering intensity I_{ss}) or contained internalized microcapsules (with high I_{ss}). Outside these borders, cellular debris, apoptotic cells and microcapsule debris are commonly found. The cells determined as being viable were re-plotted according to the emission of red (I_{red}) and green (I_{green}) fluorescence emitted by the DQ-ovalbumin (Fig. 5B). It should be noted that a cell can bear DQ-ovalbumin-loaded microcapsules in any degradation stage, that is, DQ-ovalbumin exhibiting red (intact), green (degraded) or both (in the process of degradation). Thus, a control of cells cultured without microcapsules was used to define a new area, delimited by a yellow frame in Fig. 5B, which consists of cells that neither internalized microcapsules nor exhibited intense fluorescence. Outside this area, cells containing microcapsules are identified and were thus quantified. The data indicate that 63 ± 17% of hMSCs internalized $(CHI/ELR\text{-}RGD)_2$ microcapsules (Fig. 5E). The same analysis was performed for $(CHI/ELR\text{-}RDG^{(-)})_2$ (see Fig. 5C and D), after which an internalization efficacy of 53 ± 10% was determined. No statistical differences were found between the two cases, indicating that the exhibition of RGD and $RDG^{(-)}$ has a minor influence on the incorporation of the microcapsules by hMSCs.

On internalization of a drug carrier, it is important to ensure that the agent is not only delivered, but also available for use by cells. Thanks to the use of DQ-ovalbumin, the consumption of this cargo by cells could be conveniently assessed by fluorescence changes. The bioavailability of DQ-ovalbumin was evaluated by co-incubating cultured hMSCs with each type of microcapsule in parallel for 3 h and 72 h. The schematic representation in Fig. 6A shows the various stages of enzymatic cleavage of the encapsulated protein. Until the cargo reaches a fully degraded state, the intensity of green fluorescence increases, and red decreases. Their simultaneous emission results in the orange and yellow intermediate colors observable under the fluorescence microscope.

After 3 h of incubation and a rinsing step with DPBS, few microcapsules were detected within the cells, these occurrences being mostly red or bright orange. This observation was common for both $(CHI/ELR\text{-}RGD)_2$ (Fig. 6B) and $(CHI/ELR\text{-}RDG^{(-)})_2$ microcapsules (Fig. 6D). Closer observation detects some green dots as early as after 3 h of co-incubation when using $(CHI/ELR\text{-}RGD)_2$ microcapsules (Fig. 6B): variables such as the pH and ionic strength influence the permeability of the polyelectrolyte capsules, and thus DQ-ovalbumin could still diffuse through the multilayer shell and be degraded by proteases [19]. After 72 h of co-incubation, a higher number of microcapsules were detected within the cells, in comparison with the previous time point. However, a predominant presence of "yellow" and "green" DQ-ovalbumin fluorescence

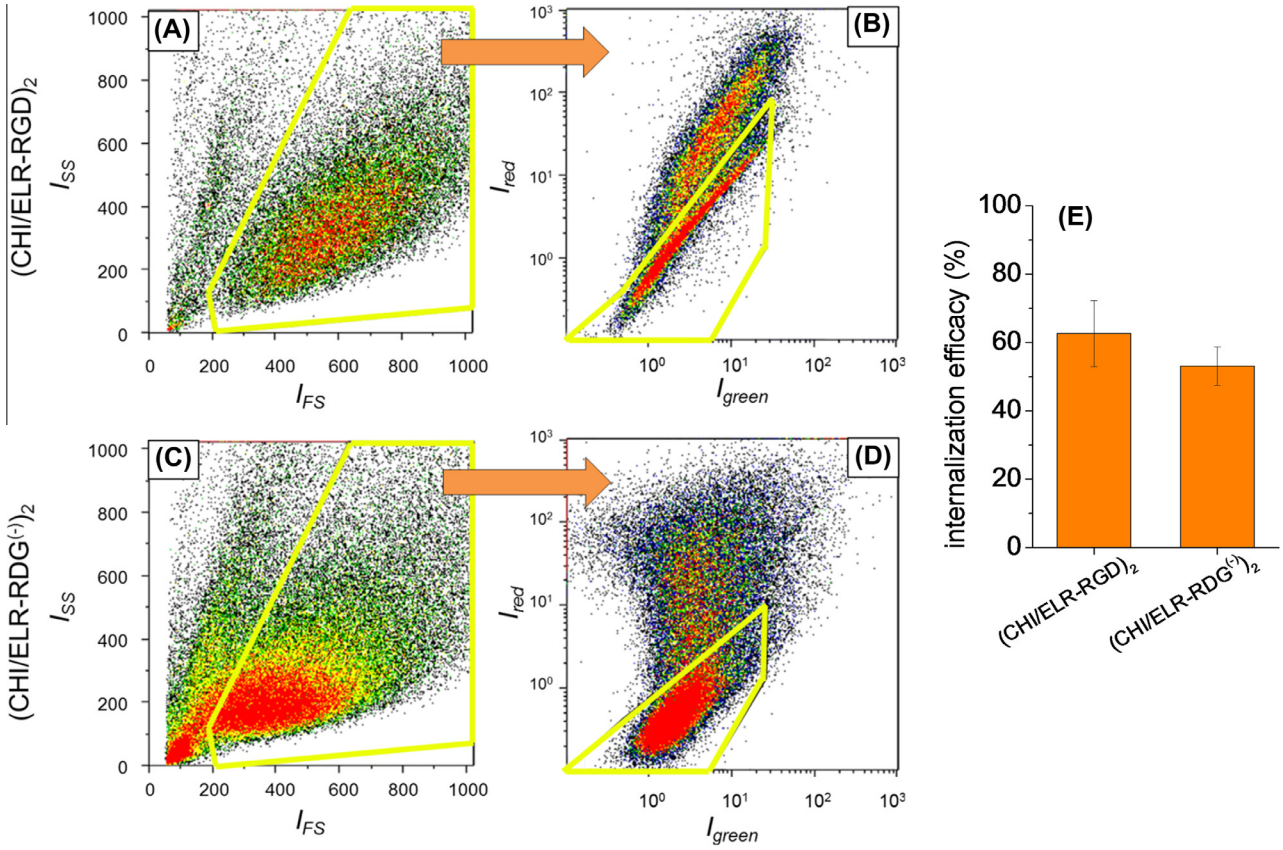

Fig. 5. Flow cytometry two-dimensional density plots of hMSCs after a 72 h incubation with (A and B) $(CHI/ELR\text{-}RGD)_2$ and (C and D) $(CHI/ELR\text{-}RDG^{(-)})_2$ microcapsules, in a ratio of 10 microcapsules per cell. The density of the events is color coded from blue (low frequency) to red (high frequency). (A and C) Side-scattering intensity (I_{SS}) is plotted as a function of forward-scattering intensity (I_{FS}). The area delimited in yellow corresponds to viable cells either empty (low I_{SS}) or with internalized microcapsules (high I_{SS}), and was established based on a control of hMSC cultured in the absence of microcapsules. (B and D) The events corresponding to viable cells were sorted according to red (I_{red}) and green (I_{green}) fluorescence intensities, and events corresponding to empty or cells containing microcapsules were subdivided. (E) Internalization efficacy of each type of capsule for three independent experiments. Data represent means of three independent experiments. Error bars represent two SD (mean ± SE). No significant statistical differences were found ($P > 0.05$).

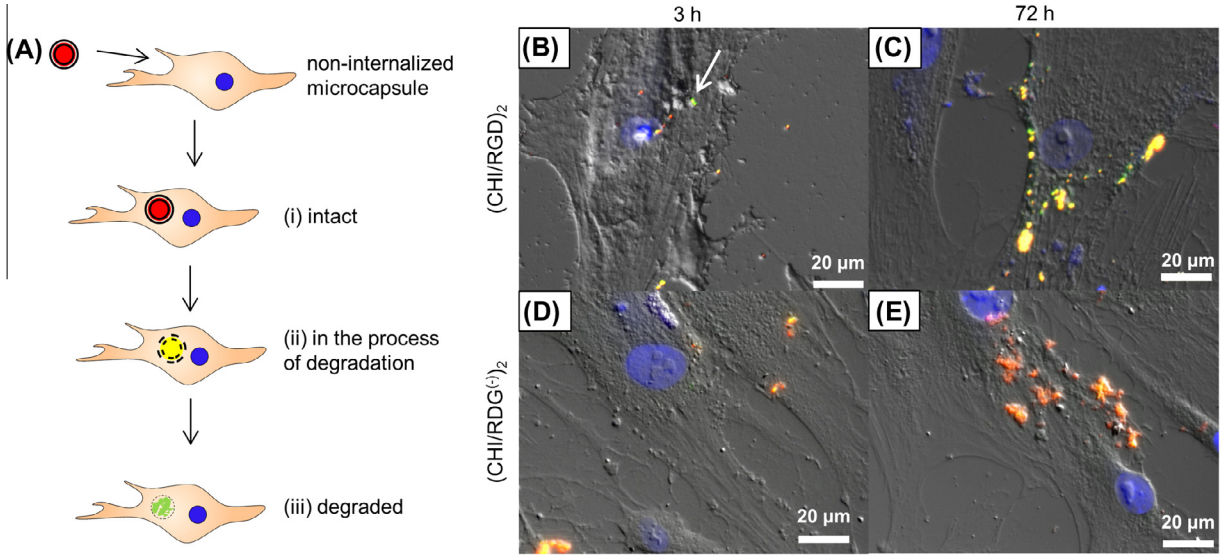

Fig. 6. Scheme (A) depicts the various degradation stages that DQ-ovalbumin undergoes. Representative microscopy images of $(CHI/ELR\text{-}RGD)_2$ and $(CHI/ELR\text{-}RDG^{(-)})_2$ microcapsules loaded with DQ-ovalbumin incubated with hMSCs (ratio 10:1) after (B and D) 3 h or (C and E) 72 h of incubation and DAPI staining (nuclei of the cells stained in blue). In B, the arrow points to a bright green spot. A shift from red/orange to green/yellow indicates a transition between fully intact to degraded cargo. Images are of fluorescence and DIC microscopy at 40× magnification.

was found inside hMSCs incubated with RGD-functionalized microcapsules (Fig. 6C), while "red" intact protein was predominant within cells incubated with $RDG^{(-)}$-functionalized microcapsules (Fig. 6E). The intense yellow and green areas in the former case show that the bioavailability of DQ-ovalbumin was higher when loaded and administered using $(CHI/ELR\text{-}RGD)_2$ microcapsules as carriers. Furthermore, the yellow intensity indicates that most of the DQ-ovalbumin was still being consumed by the hMSCs, suggesting that these microcapsules could provide sustained and long-term intracellular availability of an encapsulated active agent.

4. Discussion

Delivering an active agent to the cellular internal environment is an effective means of offering high bioavailability and efficacy. Supplying biomolecules directly to the cellular machinery has the potential to reduce drug losses significantly, compared with conventional strategies that rely on the diffusion of an agent to the surroundings of cells. For this purpose, multilayer microcapsules functionalized with ELRs were developed. This class of recombinant polypeptides is an elegant alternative to conventional multilayer formulations used to fabricate microcapsules (e.g. poly(styrene sulfonate) (PSS) and poly(allylamine hydrochloride) (PAH)). Herein, ELRs exhibiting either RGD or $RDG^{(-)}$ motifs were used. Unlike RGD, $RDG^{(-)}$ is a non-bioactive motif, similar to RGD in all aspects. $RGD^{(-)}$ differs in the position of the G and D amino acids and was previously shown to trigger significantly less cellular adhesion [39,40]. It was thus expected that the same tendency would be verified in respect of cellular uptake of this type of microcapsule. To determine that, the internalization efficacy of RGD-functionalized capsules was assessed, compared with $RDG^{(-)}$-based ones, and the role of bioactive motifs in the studied delivery mechanism was evaluated.

The first step was to assess the structure of the microcapsules produced. For the proof of concept, two bilayers were chosen, since they resulted in stable microcapsules in the shortest construction time possible. In Fig. 1, the successful production of hollow microcapsules destitute of the $CaCO_3$ template is demonstrated, and this accounts for the robustness of the synthesized structures. In particular, $(CHI/ELR\text{-}RGD)_2$ (Fig. 1C) and $(CHI/ELR\text{-}RDG^{(-)})_2$ (Fig. 1D) microcapsules—also shown in Fig. 1A—were similar in size and morphology. Since both microcapsule types were identical, any difference in internalization efficacy would be the result of the peptide sequence bioactivity rather than of morphological discrepancy. Applications that require cellular uptake and survivability also require the synthesis of separate and individual carriers, but the preparation of individual polymeric capsules while avoiding aggregation has been reportedly difficult to standardize. The present results did not reveal signs of major aggregation (refer also to Fig. B2, Appendix B), confirming that the operational conditions enabled appropriate individual spherical microstructures to be obtained for studies involving the internalization of microcarriers.

The hMSCs were used to show the internalization of ELR-functionalized microcapsules. MSCs are hypoimmunogenic and pluripotent cells able to differentiate in vitro, ex vivo and in vivo in multiple cell types. These characteristics have been considered crucial factors in developing new candidates for clinical use, especially in tissue engineering and regenerative medicine applications, such as transplantation, local implantation, gene therapy and drug delivery [41,42]. Cellular therapies, in particular, can be envisaged, where bioactive molecules are internalized with the aim of controlling cellular behavior, such as the induced differentiation of MSCs into osteoblasts [43]. Therefore, although the differentiation of stem cells was not envisaged in the context of this work, the option to study hMSCs in a model for internalization opens the possibility to use ELR-based microcapsules in therapies involving stem cells.

Considering the use of these microcapsules in biological applications, it was important to assess whether the microcapsules were harmful to hMSCs. The metabolic activity in vitro is presented in Fig. 2. The results demonstrate that it is possible to apply relatively large amounts of microcapsules to hMSCs without severely affecting their viability. LIVE/DEAD® assays were in accordance with these results, showing that the contact with microcapsules did not cause harm to hMSCs and that they could be cultured for longer times after a co-incubation period of 3 days (Fig. 3). Nonetheless, the results revealed the occurrence of three trends. The first trend is that cell viability was higher than 100% in the lowest microcapsule/cell ratios. Analogous viability increments in cell cultures incubated with ELRs nano-/micro-particles evaluated through different metabolic activity tests were described previously [44,45]. The second is a tendency for metabolic activity to decrease for higher ratios (higher than 50:1 for $(CHI/ELR\text{-}RGD)_2$ and 60:1 for $(CHI/ELR\text{-}RDG^{(-)})_2$ microcapsules). Although these microcapsules were non-cytotoxic towards hMSCs (even for the highest studied ratios), a large number of microcapsules may have a negative impact in the metabolic activity of the cells. This tendency could be explained by the accumulation of microcapsules on top of the cells and the increasing number of carriers that contain polycationic species (CHI) as building blocks [46,47]. In fact, the lowest microcapsule/cell ratios were those providing the most favorable conditions for hMSC co-incubation. For this reason, a ratio of 10:1 was used in every subsequent experiment, including LIVE/DEAD® assays. The third trend is that RGD-functionalized microcapsules provided an overall bioactivity higher than their non-functional analogues. Though not statistically significant, this small disparity could be the result of RGD-induced integrin activation in the dorsal region of the cells. This interaction is known to be involved in several metabolic pathways, such as those of proliferation and differentiation [48,49].

Flow cytometry was employed to quantify the internalization efficacy of RGD- and $RDG^{(-)}$-functionalized microcapsules (Fig. 5). The percentage of cells containing microcapsules after 72 h of co-incubation was not significantly different, suggesting that the internalization of LbL microcapsules is not affected when coupled with biofunctional components. Previously, Caruso and coworkers [50] showed that PSS/PAH capsules (~500 nm) functionalized with humanized A33 monoclonal antibodies could be internalized specifically by LIM1215 colorectal cancer cells. However, in another work, De Koker et al. [51] inhibited different endocytic pathways and actin polymerization in bone-marrow-derived dendritic cells. Their results demonstrated that microcapsules ~3 μm are internalized via macropinocytosis—a non-specific endocytosis mechanism for foreign materials with roughly 500–2000 nm [52]. Given the dimensions of the capsules studied herein, it is possible that macropinocytosis was the major endocytosis mechanism involved in the cellular uptake of ELR-based carrier devices of micrometric dimensions, to which surface functionalization with RGD or $RDG^{(-)}$ did not play a determinant role.

One may also reflect on the negative charge exhibited by the ELR outer layer, which could potentially hinder the internalization by conflicting with the electrostatic nature of the cellular membrane [53]. However, electrostatic interactions alone were previously unable to account for cellular adhesion to surfaces modified with polycations [54] and thus are expected to have little influence in comparison with the bioactive properties of the macromolecules used.

Although both types of microcapsules were internalized with similar efficacy, the cellular consumption of the encapsulated DQ-ovalbumin was markedly distinct. The microscopy comparison (Fig. 6) shows that both $(CHI/ELR\text{-}RGD)_2$ and $(CHI/ELR\text{-}RDG^{(-)})_2$

situations bear little difference in respect of the number of internalized carriers, but a dominant emission fluorescence towards the green spectrum—that of cleaved DQ-ovalbumin—was dominant in the former. First, the fact that this cargo remained well protected after 72 h of co-incubation in both cases (judging by the yellow and red intensities in Fig. 6C and E, respectively) could be useful, especially when an agent needs to be delivered in small and controlled doses over time: for example, for the orderly differentiation of stem cells, considering the cells used in this internalization model. Second, the cargo entrapped in RGD-functionalized microcapsules was cleaved faster than when entrapped in $RDG^{(-)}$-functionalized ones, evidencing higher bioavailability of DQ-ovalbumin when encapsulated in the former carrier type. In this sense, the cargo bioavailability does not seem to match the cellular uptake results: the internalization efficacy was not influenced significantly by the ELR functionalization, whereas the intracellular processing of the cargo was. It is true that the role of macropinocytosis was demonstrated previously, but the fate of the cargo afterwards has not usually been studied. Given that surface functionalization had little influence on the internalization efficacy, one would expect that the degradation rate of their cargo would be similar. In light of these results, it could be suggested that the distinct functionality of the adsorbed recombinamers triggers distinct proteolytic pathways, based on accounts that relate RGD to (i) the activation of proliferation- and differentiation-related integrins [55], and (ii) increased endosomal trafficking [35,36,56,57]. However, the study of such mechanisms was not in the scope of this work, but ensuring that drugs can be consumed by cells after internalization is an important issue. Therefore, such mechanisms should be studied in the future in order to properly determine the fate of cargo on cellular uptake, using in particular carriers of the same class internalized by similar endocytic mechanisms.

5. Conclusions

The fabrication of multilayer microcapsules made of natural and nature-inspired polymers for intracellular delivery of active agents was presented. Thanks to the nature of the constituents, high quantities of microcapsules were shown to be non-cytotoxic for the cells. Cellular uptake was demonstrated, showing their potential as carriers for drug delivery directly to the cellular machinery. In the future, this delivery path may help to minimize drug losses and increase their delivery control and efficacy. The internalization efficacy demonstrated for hMSCs shows promise for their use in cell/tissue engineering and regenerative medicine, where it is important to control the differentiation of stem cells into specific phenotypes. This work confirmed that CHI/ELR microcapsules could interact and be internalized by cells, but experiments with microcapsules loaded with actual active agents, such as molecules that trigger the differentiation of cells into specific phenotypes, are envisaged. The mechanism of internalization of the microcapsules at this scale did not depend on the surface functionalization. In this context, the recombinant nature of ELRs will be of interest for further study of the microcapsule endocytosis mechanism. In particular, it is possible that the production of smaller capsules using nanotemplates may increase the influence of RGD and facilitate internalization [58]. The inclusion of bioactive motifs other than this generic motif may constitute a strong advantage in using such recombinant technologies, allowing exploration not only of specific recognition processes, but also of degradation pathways for targeted delivery and increased drug efficacy. Therefore, multilayer microcapsules using biomimetic ingredients for intracellular delivery are promising new strategies for increasing the availability of molecules of interest in cells and for targeted biomedical applications.

Acknowledgements

The authors acknowledge financial support from Fundação para a Ciência e Tecnologia (Grant SFRH/BD/61126/2009), "Fundo Social Europeu", "Programa Diferencial de Potencial Humano", EU 7th Framework Programme (No. REGPOT-CT2012-316331-POLARIS), the EU through the European Regional Development Fund (ERDF), from the MINECO (MAT-2010-15982, MAT2010-15310, PRI-PIBAR-2011-1403 and MAT2012-38043), the JCyL (projects VA049A11, VA152A12 and VA155A12), the CIBER-BBN, and the Instituto de Salud Carlos III under the "Network Center of Regenerative Medicine and Cellular Therapy of Castilla and Leon".

References

[1] Lima AC, Sher P, Mano JF. Production methodologies of polymeric and hydrogel particles for drug delivery applications. Exp Opin Drug Deliv 2012;9:231–48.
[2] Malam Y, Loizidou M, Seifalian AM. Liposomes and nanoparticles: nanosized vehicles for drug delivery in cancer. Trends Pharmacol Sci 2009;30:592–9.
[3] Meng F, Zhong Z, Feijen J. Stimuli-responsive polymersomes for programmed drug delivery. Biomacromolecules 2009;10:197–209.
[4] Szarpak A, Cui D, Dubreuil F, De Geest BG, De Cock LJ, Picart C, et al. Designing hyaluronic acid-based layer-by-layer capsules as a carrier for intracellular drug delivery. Biomacromolecules 2010;11:713–20.
[5] Caruso F, Caruso RA, Möhwald H. Nanoengineering of inorganic and hybrid hollow spheres by colloidal templating. Science 1998;282:1111–4.
[6] De Cock LJ et al. Polymeric multilayer capsules in drug delivery. Angew Chem Int Ed 2010;49:6954–73.
[7] del Mercato LL et al. LbL multilayer capsules: recent progress and future outlook for their use in life sciences. Nanoscale 2010;2:458–67.
[8] Petrov AI, Volodkin DV, Sukhorukov GB. Protein—calcium carbonate coprecipitation: a tool for protein encapsulation. Biotechnol Prog 2005;21:918–25.
[9] Tong W, Zhu Y, Wang Z, Gao C, Möhwald H. Micelles-encapsulated microcapsules for sequential loading of hydrophobic and water-soluble drugs. Macromol Rapid Commun 2010;31:1015–9.
[10] Gribova V, Auzely-Velty R, Picart C. Polyelectrolyte multilayer assemblies on materials surfaces: from cell adhesion to tissue engineering. Chem Mater 2011;24:854–69.
[11] Shukla A, Avadhany SN, Fang JC, Hammond PT. Tunable vancomycin releasing surfaces for biomedical applications. Small 2010;6:2392–404.
[12] Tang Z, Wang Y, Podsiadlo P, Kotov NA. Biomedical applications of layer-by-layer assembly: from biomimetics to tissue engineering. Adv Mater 2006;18:3203–24.
[13] Costa RR, Custódio CA, Arias FJ, Rodríguez-Cabello JC, Mano JF. Nanostructured and thermoresponsive recombinant biopolymer-based microcapsules for the delivery of active molecules. Nanomedicine NBM 2013;9:895–902.
[14] Facca S et al. Active multilayered capsules for in vivo bone formation. Proc Natl Acad Sci USA 2010;107:3406–11.
[15] McShane M, Ritter D. Microcapsules as optical biosensors. J Mater Chem 2010;20:8189–93.
[16] Shimoni O, Yan Y, Wang Y, Caruso F. Shape-dependent cellular processing of polyelectrolyte capsules. ACS Nano 2012;7:522–30.
[17] Tong W, She S, Xie L, Gao C. High efficient loading and controlled release of low-molecular-weight drugs by combination of spontaneous deposition and heat-induced shrinkage of multilayer capsules. Soft Matter 2011;7:8258–65.
[18] Su X, Kim B-S, Kim SR, Hammond PT, Irvine DJ. Layer-by-layer-assembled multilayer films for transcutaneous drug and vaccine delivery. ACS Nano 2009;3:3719–29.

[19] Rivera-Gil P, De Koker S, De Geest BG, Parak WJ. Intracellular processing of proteins mediated by biodegradable polyelectrolyte capsules. Nano Lett 2009;9:4398–402.
[20] Nel AE et al. Understanding biophysicochemical interactions at the nano-bio interface. Nat Mater 2009;8:543–57.
[21] Panyam J, Labhasetwar V. Biodegradable nanoparticles for drug and gene delivery to cells and tissue. Adv Drug Deliv Rev 2003;55:329–47.
[22] Patri AK, Kukowska-Latallo JF, Baker Jr JR. Targeted drug delivery with dendrimers: comparison of the release kinetics of covalently conjugated drug and non-covalent drug inclusion complex. Adv Drug Deliv Rev 2005;57:2203–14.
[23] Wei H, Zhuo R-X, Zhang X-Z. Design and development of polymeric micelles with cleavable links for intracellular drug delivery. Prog Polym Sci 2013;38:503–35.
[24] Volodkin DV, Larionova NI, Sukhorukov GB. Protein encapsulation via porous CaCO3 microparticles templating. Biomacromolecules 2004;5:1962–72.
[25] Correia CR, Reis RL, Mano JF. Multilayered hierarchical capsules providing cell adhesion sites. Biomacromolecules 2013;14:743–51.
[26] She Z, Antipina MN, Li J, Sukhorukov GB. Mechanism of protein release from polyelectrolyte multilayer microcapsules. Biomacromolecules 2010;11:1241–7.
[27] Angelatos AS, Katagiri K, Caruso F. Bioinspired colloidal systems via layer-by-layer assembly. Soft Matter 2006;2:18–23.
[28] Rinaudo M. Chitin and chitosan: properties and applications. Prog Polym Sci 2006;31:603–32.
[29] Urry DW. What sustains life? A consilient mechanism for protein-based machines and materials. New York: Springer; 2006.
[30] Girotti A, Fernández-Colino A, López IM, Rodríguez-Cabello JC, Arias FJ. Elastin-like recombinamers: biosynthetic strategies and biotechnological applications. Biotechnol J 2011;6:1174–86.
[31] Nettles DL, Chilkoti A, Setton LA. Applications of elastin-like polypeptides in tissue engineering. Adv Drug Deliv Rev 2010;62:1479–85.
[32] Costa RR, Testera AM, Arias FJ, Rodríguez-Cabello JC, Mano JF. Layer-by-layer film growth using polysaccharides and recombinant polypeptides: a combinatorial approach. J Phys Chem B 2013;117:6839–48.
[33] Hynes RO. Integrins: bidirectional, allosteric signaling machines. Cell 2002;110:673–87.
[34] Hu Z et al. Arg-Gly-Asp (RGD) peptide conjugated poly(lactic acid)–poly(ethylene oxide) micelle for targeted drug delivery. J Biomed Mater Res A 2008;85A:797–807.
[35] Oba M et al. Polyplex micelles with cyclic RGD peptide ligands and disulfide cross-Links directing to the enhanced transfection via controlled intracellular trafficking. Mol Pharm 2008;5:1080–92.
[36] Xiong X-B, Mahmud A, Uludağ H, Lavasanifar A. Multifunctional polymeric micelles for enhanced intracellular delivery of doxorubicin to metastatic cancer cells. Pharm Res 2008;25:2555–66.
[37] Signini R, Campana Filho SP. On the preparation and characterization of chitosan hydrochloride. Polym Bull 1999;42:159–66.
[38] Semmling M, Kreft O, Muñoz Javier A, Sukhorukov GB, Käs J, Parak WJ. A novel flow-cytometry-based assay for cellular uptake studies of polyelectrolyte microcapsules. Small 2008;4:1763–8.
[39] Costa RR, Custódio CA, Arias FJ, Rodríguez-Cabello JC, Mano JF. Layer-by-layer assembly of chitosan and recombinant biopolymers into biomimetic coatings with multiple stimuli-responsive properties. Small 2011;7:2640–9.
[40] Liu JC, Tirrell DA. Cell response to RGD density in cross-linked artificial extracellular matrix protein films. Biomacromolecules 2008;9:2984–8.
[41] Pittenger MF et al. Multilineage potential of adult human mesenchymal stem cells. Science 1999;284:143–7.
[42] Uccelli A, Moretta L, Pistoia V. Mesenchymal stem cells in health and disease. Nat Rev Immunol 2008;8:726–36.
[43] Oliveira JM, Kotobuki N, Tadokoro M, Hirose M, Mano JF, Reis RL, et al. Ex vivo culturing of stromal cells with dexamethasone-loaded carboxymethylchitosan/poly(amidoamine) dendrimer nanoparticles promotes ectopic bone formation. Bone 2010;46:1424–35.
[44] Bessa PC et al. Thermoresponsive self-assembled elastin-based nanoparticles for delivery of BMPs. J Controlled Release 2010;142:312–8.
[45] Dash BC, Mahor S, Carroll O, Mathew A, Wang W, Woodhouse KA, et al. Tunable elastin-like polypeptide hollow sphere as a high payload and controlled delivery gene depot. J Controlled Release 2011;152:382–92.
[46] De Koker S et al. In vivo cellular uptake, degradation, and biocompatibility of polyelectrolyte microcapsules. Adv Funct Mater 2007;17:3754–63.
[47] Kirchner C, Javier AM, Susha AS, Rogach AL, Kreft O, Sukhorukov GB, et al. Cytotoxicity of nanoparticle-loaded polymer capsules. Talanta 2005;67:486–91.
[48] Ivaska J, Heino J. Interplay between cell adhesion and growth factor receptors: from the plasma membrane to the endosomes. Cell Tissue Res 2010;339:111–20.
[49] Johnson MS, Lu N, Denessiouk K, Heino J, Gullberg D. Integrins during evolution: evolutionary trees and model organisms. Biochim Biophys Acta Biomembr 2009;1788:779–89.
[50] Cortez C et al. Targeting and uptake of multilayered particles to colorectal cancer cells. Adv Mater 2006;18:1998–2003.
[51] De Koker S et al. Polyelectrolyte microcapsules as antigen delivery vehicles to dendritic cells: uptake, processing, and cross-presentation of encapsulated antigens. Angew Chem Int Ed 2009;48:8485–9.
[52] Bishop NE. An update on non-clathrin-coated endocytosis. Rev Med Virol 1997;7:199–209.
[53] Ke J-H, Young T-H. Multilayered polyplexes with the endosomal buffering polycation in the core and the cell uptake-favorable polycation in the outer layer for enhanced gene delivery. Biomaterials 2010;31:9366–72.
[54] Lee H-S, Eckmann DM, Lee D, Hickok NJ, Composto RJ. Symmetric pH-dependent swelling and antibacterial properties of chitosan brushes. Langmuir 2011;27:12458–65.
[55] Adams JC, Watt FM. Changes in keratinocyte adhesion during terminal differentiation: reduction in fibronectin binding precedes α5β1 integrin loss from the cell surface. Cell 1990;63:425–35.
[56] Fang IJ, Slowing II, Wu KCW, Lin VSY, Trewyn BG. Ligand conformation dictates membrane and endosomal trafficking of arginine–glycine–aspartate (RGD)-functionalized mesoporous silica nanoparticles. Chem Eur J 2012;18:7787–92.
[57] Shayakhmetov DM, Eberly AM, Li Z-Y, Lieber A. Deletion of penton RGD motifs affects the efficiency of both the internalization and the endosome escape of viral particles containing adenovirus serotype 5 or 35 fiber knobs. J Virol 2005;79:1053–61.
[58] Rejman J, Oberle V, Zuhorn IS, Hoekstra D. Size-dependent internalization of particles via the pathways of clathrin- and caveolae-mediated endocytosis. Biochem J 2004;377:159–69.